Wang *et al. PhotoniX* (2022) 3:10
https://doi.org/10.1186/s43074-022-00057-1

PhotoniX

RESEARCH Open Access

Metasurface with dynamic chiral meta-atoms for spin multiplexing hologram and low observable reflection

He Wang[1,2†], Zhe Qin[1†], Lingling Huang[2*], Yongfeng Li[1*], Ruizhe Zhao[2], Hongqiang Zhou[2], Haoyang He[2], Jieqiu Zhang[1] and Shaobo Qu[1]

*Correspondence: huanglingling@bit.edu.cn; liyf217130@126.com
†He Wang and Zhe Qin contributed equally to this work.
[1] Department of Basic Sciences, Air Force Engineering University, Xi'an 710051, Shaanxi, China
[2] Beijing Engineering Research Center of Mixed Reality and Advanced Display, School of Optics and Photonics, Beijing Institute of Technology, Beijing 100081, China

Abstract

Spin light manipulation based on chiral metasurfaces is a striking hotspot that has intrigued huge attention. Circular dichroism, a unique phenomenon of chiral atoms/molecules, has been regarded as another auxiliary dimension for guiding electromagnetic waves, which has been explored in the field of artificial material sciences yet a challenging issue. Here, a generic strategy based on dynamic chiral meta-atom for revealing strong circular dichroism as well as applicable electromagnetic functionality is proposed in microwave regime. We demonstrate a dynamic metasurface that enables the fully independent holograms reconstruction for one circular polarization or the other at the active operating state. On the other hand, the electromagnetic scattering is realized for lowering observable backward reflection at the passive state. Numerical simulation and experimental verification are conducted to manifest the feasibility. It is expected that the proposed strategy can be applied to broaden the horizon for dynamic chiral meta-devices and may find applications in information encryption, anti-counterfeiting, and other dynamic systems.

Introduction

In the past few decades, metasurfaces have attracted huge amounts of discussion in a wide variety of academic and engineering disciplines due to their powerful capabilities of tailoring light [1–4]. Generally, metasurfaces are composed of meta-atoms in deep subwavelength scale with periodic or quasi-periodic arrangements [5]. By exploiting the potential of metasurfaces in electromagnetic manipulation, a large number of unparalleled phenomena and devices have become to emerge, including anomalous reflection/refraction [6, 7], vortex beam generation [8, 9], polarization conversion [10], metalens [11, 12], perfect absorber [13], meta-holograms [14–17], and the like.

From the perspective of geometry structure, the categories of meta-atom can be summarized as mirror symmetry, rotational symmetry, and chirality. In general, the absence of mirror symmetry in metasurfaces building blocks renders chirality [18]. Chiral structures are considered to interact differently with different input spin states and the optical responses that are sensitive to handedness are called

Springer Open

© The Author(s) 2022. **Open Access** This article is licensed under a Creative Commons Attribution 4.0 International License, which permits use, sharing, adaptation, distribution and reproduction in any medium or format, as long as you give appropriate credit to the original author(s) and the source, provide a link to the Creative Commons licence, and indicate if changes were made. The images or other third party material in this article are included in the article's Creative Commons licence, unless indicated otherwise in a credit line to the material. If material is not included in the article's Creative Commons licence and your intended use is not permitted by statutory regulation or exceeds the permitted use, you will need to obtain permission directly from the copyright holder. To view a copy of this licence, visit http://creativecommons.org/licenses/by/4.0/.

chiroptical responses [19]. With the assistance of metasurfaces, the weak chiroptical effects in nature materials can be strikingly revealed and enhanced by artificially arranged meta-atoms [20–22]. Among them, the differential extinction for left-handed circular polarization (LHCP) state and right-handed circular polarization (RHCP) state can be achieved as circular dichroism by the meticulous design of geometric chirality [23–28]. Unlike the flat metallic sheets that reflect circularly polarized waves with reverse handedness, the chiral metasurfaces selectively reflect one of the circularly polarized waves without changing the handedness, while the other is absorbed [29]. On the other hand, chiral structures possess the potential to acquire circular polarization conversion, and thereafter governed by Pancharatam-Berry (PB) phase principle [30]. To date, introducing three-dimensional or cascaded structures are effective methods to achieve circular dichroitic responses in a large portfolio of designs and spanned the frequencies from visible to gigahertz (GHz) [31–33]. Nevertheless, this happens at the expense of complex fabrication schemes and limited reconfigurability.

With the increasing demands of modern encrypted communication and anti-counterfeiting technology, a tunable or dynamic strategy aiming to provide a platform for achieving more flourishing applications and functionalities is urgent. Although the explorations of metasurfaces are widely reported so far, most of them are passive with fixed functionality and suffer from limited flexibility [34]. Fortunately, the dynamic counterparts by loading active elements have been proposed to improve the limitation, which are demonstrated to offer effective manner to vary the electromagnetic response of meta-atoms, thereafter achieving dynamic functionality variations [35–39]. This approach presents great potential for anti-jam and capacity expansion, especially for the microwave regime. Therefore, it is enlightening to dynamically achieve circular dichroism as an auxiliary dimension of electromagnetic manipulation and simultaneously integrate multiple functionalities within a single aperture. However, the research of this academic issue still needs to be further explored.

Here, we propose a generic strategy to achieve dynamic control of electromagnetic waves for spin multiplexing hologram and low observable reflection by an active manner. By introducing varistor diode into the split-ring metallic resonator at mirror-symmetrical/chiral positions, the proposed meta-atom can be used to dynamically achieve electromagnetic wave absorption of both spin states and circular dichroitic effect. Accordingly, the amplitude-based spin multiplexing hologram for reconstructing images for either left-handed or right-handed circularly polarized waves are presented by bias voltage driven. On the other hand, the amplitude distribution becomes uniform without the excitation of voltage. Accordingly, the phase difference of π of distinct meta-atoms can be correlated to the coding metasurface principle. Thereafter, the low observable reflection of beam scattering can be obtained. The fabricated prototype with 60×60 pixels demonstrates the feasibility of our proposed voltage-driven chiral metasurface. Encouragingly, the proposed paradigm offers additional dynamic strategy to push the circular dichroitic metasurface to application level, which possesses great potential in the fields of information encryption, anti-counterfeiting, and stealth.

Methods

Figure 1 presents the conceptual illustration of the proposed voltage-driven chiral metasurface. A pair of electrodes are set at two sides of the metasurface to achieve series feed, which can efficiently achieve dynamic control without extra feed network. Based on the circular dichroitic effect of meta-atoms, the independent amplitude distributions (defined as L-code and R-code) can be obtained with left-handed and right-handed circularly polarized waves illuminating when the varistor diodes are operated at "On" states. Moreover, the proposed chiral metasurface becomes passive type when the varistor diodes are at "Off" states. Thus, the amplitude coding distributions become suppressed and the phase responses become the dominant effect to reveal low observable reflection.

The proposed chiral metasurface is fabricated by printed circuit board (PCB) technique which consists of 60 × 60 meta-atoms with the total size of 385 mm × 360 mm (including the feeding parts set at two sides of the fabricated prototype) that are fed in series in each row. The metallic structure of split-ring resonator and metallic back sheet are made of copper with the thickness of 0.02 mm and the conductivity of 5.8×10^7 S/m. The dielectric spacer F4B (the relative permittivity of 2.65 and the loss tangent of 0.001) with the thickness of 3.0 mm is applied to adapt the design. The varistor diodes (type of BAP70–02, with the total number of 3672) are loaded into the gaps of split-ring resonators, which can be controlled by the direct current (DC) bias voltage excitation. The inductances (type of LQW18AN27NGOOD, with the total number of 3600) are loaded into the gaps of series wires to introduce a radio-frequency choke, which blocks alternating current but allows direct current to pass through. In this way, the electromagnetic properties of the metasurface are relatively stable when driven by external voltage.

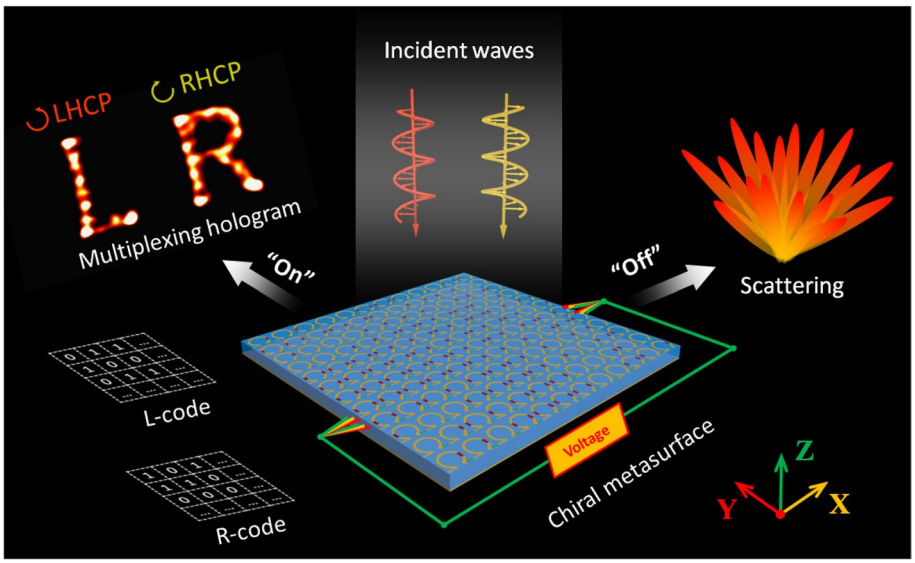

Fig. 1 Conceptual illustration of the proposed voltage-driven chiral metasurface

Results

To achieve circular dichroism, it is necessary to simultaneously break the n-fold rotational ($n>2$) and mirror symmetries for a two-dimensional meta-atom [40]. However, the symmetry-breaking effect for circular dichroism in microwave frequency is relatively slight due to the inadequate losses of metal and substrate, especially for the meta-atoms of planar version. In order to reveal conspicuous circular dichroism and thereafter promote it to the application level of electromagnetic manipulation in microwave regime, we conduct the strategy of introducing Ohmic dissipation into the chiral position of meta-atom. In this design, four kinds of meta-atoms with the same framework but different to the varistor diode loading positions are implemented, which are shown in Fig. 2

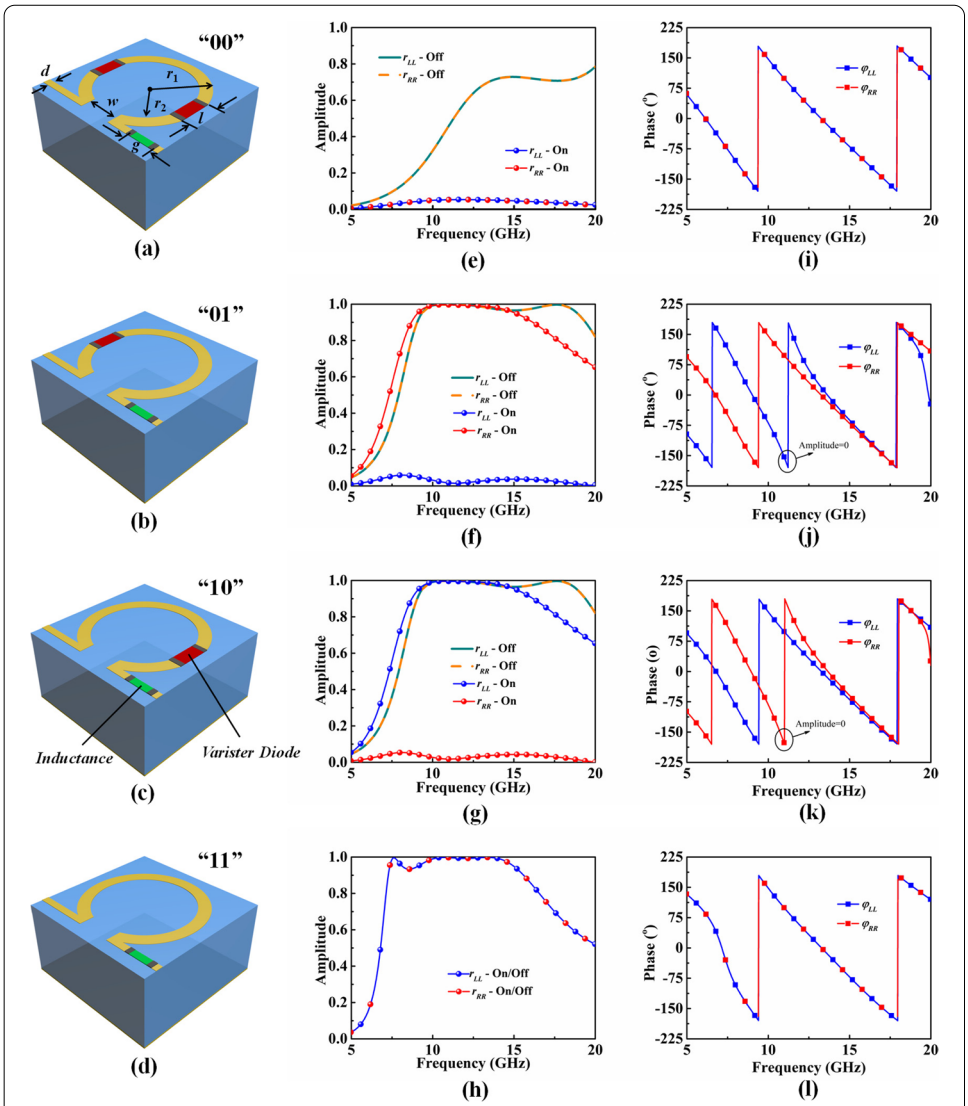

Fig. 2 (**a**)-(**d**) The proposed four kinds of meta-atoms. The parameters are optimized as: the periodical length of 6.0 mm, $r_1=2.5$ mm, $r_2=2.0$ mm, $l=1.4$ mm, $g=1.2$ mm, and $d=0.3$ mm. (**e**)-(**h**) Amplitude responses of the four kinds of meta-atom. r_{LL} and r_{RR} represent the co-polarized amplitude under the incidence of left-handed and right-handed circularly polarized waves. (**i**)-(**l**) Phase responses of the four kinds of meta-atom when varistor diodes are operated at "On" states. The φ_{LL} and φ_{RR} represent the phase of output co-polarized component under the incidence of left-handed and right-handed circularly polarized waves

(**a**)-(**d**). According to the amplitude responses to the left-handed and right-handed circularly polarized waves, we use binary codes to define these meta-atoms as "00", "01", "10", and "11", respectively. Here, the first bit of "0" or "1" represents the absorption or reflection of left-handed circularly polarized waves. The second bit of "0" or "1" represents the absorption or reflection of right-handed circularly polarized waves. The electromagnetic properties of the meta-atoms are simulated by computer simulation technology (CST) Microwave Studio. The periodic boundary conditions of "Unit cell" are applied in both x- and y-directions, while two Flouquet ports are fixed at $\pm z$ directions.

The amplitude curves of the corresponding meta-atoms are depicted in Fig. 2 (**e**)-(**h**), in which the cases of varistor diode at "On" and "Off" states are compared. For the varistor diode, the resistance is 150 Ω when driven by DC bias voltage at "On" state, while it becomes 200 MΩ at "Off" state. It is observed that the "00" and "11" meta-atoms have the same amplitude responses to the incidence of circularly polarized waves with different spin states no matter the varistor diodes are at "On" or "Off" states. However, the amplitude responses of both spin states are sharply suppressed for "00" meta-atom when the loaded varistor diodes are at "On" states. On the contrary, the "01" and "10" meta-atoms reveal conspicuous circular dichroitic effect when the varistor diodes are at "On" states. The "01" meta-atom achieves the absorption of left-handed circularly polarized reflection; the "10" meta-atom obtains the absorption of right-handed circularly polarized reflection. Nevertheless, the circular dichroitic effects disappear when the varistor diodes are at "Off" states. Instead, the reflected amplitude responses of both spin states are nearly 1 in 8–18 GHz. Noticed that the meta-atoms of "00" and "11" satisfy the requirements of simultaneously breaking the n-fold rotational ($n > 2$) and mirror symmetries within planar version (the positions of loading inductances break the symmetries), but the expected depression of circular dichroitic effects are acquired. These phenomena are caused by the ohmic dissipations of the used inductances are very small that can hardly enhance the chirality. The phase responses are shown in Fig. 2 (**i**)-(**l**), in which the varistor diodes are at "On" states. Obviously, the phase responses of "00" and "11" meta-atoms are insensitive to the spin states, and the phase responses of these two kinds of meta-atom are almost the same within 8–20 GHz. Moreover, it is noticed that there are phase differences between the spin states with the amplitude responses equal to 0 (ϕ_{LL} for "01"; ϕ_{RR} for "10") and the other of "01" and "10" meta-atoms. But for the amplitude holographic metasurface, these phase differences can hardly influence on the reconstructed images. Therefore, the phase deviations can be ignored for the spin multiplexing design.

On the other hand, the phase responses of left-handed and right-handed circular polarization with the varistor diodes at "Off" states are compared in Fig. 3. In this case, the metallic resonances become the dominant contribution to the electromagnetic characteristics of meta-atoms. It can be observed in Fig. 3(**a**) that the phase differences are about 180° between "00"/"01" and "10"/"11" meta-atoms in the frequency band of 8 GHz to 18 GHz for left-handed circular polarization. Similarly, the phase differences are about 180° between "00"/"10" and "01"/"11" meta-atoms within the same frequency band for right-handed circular polarization. Furthermore, the amplitude responses of the four kinds of meta-atom are larger than 0.75 in 13–17 GHz, thus the phase coding sequences can be theoretically implemented for "Off" states.

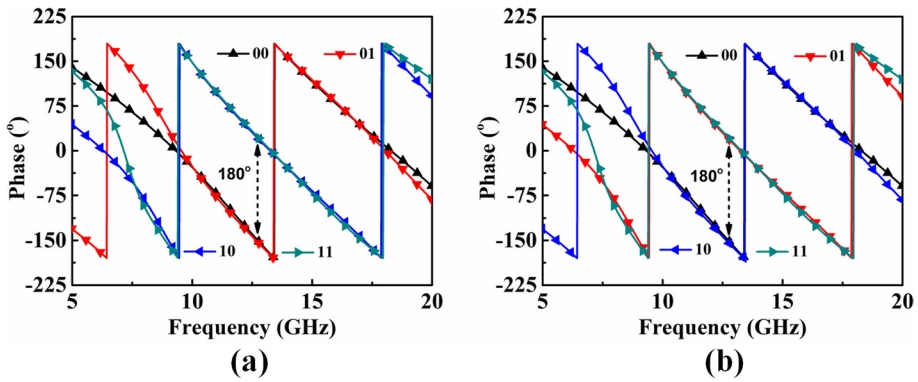

Fig. 3 Phase responses of the four kinds of meta-atom when varistor diodes are operated at "Off" states. (**a**) Left-handed polarized waves. (**b**) Right-handed polarized waves

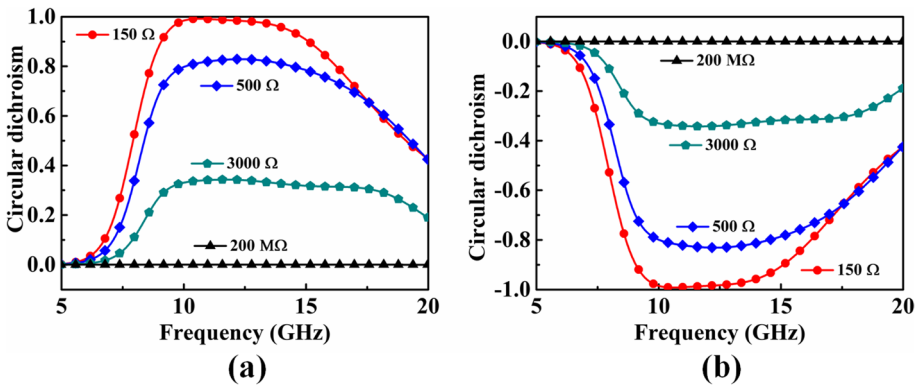

Fig. 4 Circular dichroism curves with different Ohmic dissipations. (**a**) "01" meta-atom. (**b**) "10" meta-atom

Considering that the resistance value of varistor diode is gradually changed when driven by different bias voltage. Here, the circular dichroism characteristics of the "01" and "10" meta-atoms under the different resistance value are explored, as shown in Fig. 4(a) and Fig. 4(b). Circular dichroism is the difference between the absorption of left-handed and right-handed circularly polarized waves, which can be calculated as [41]:

$$CD = A_{LHCP} - A_{RHCP}, \tag{1}$$

where the corresponding absorption is governed by $A_{LHCP(RHCP)} = 1\text{-}|r_{LL}\ (_{RR})|^2\text{-}|r_{RL}\ (_{LR})|^2$, r_{RL} and r_{LR} are the cross-polarized amplitude of left-handed and right-handed circularly polarized waves, respectively. It can be seen that the strong circular dichroitic effects are achieved when the varistor diodes are driven by bias voltage at "On" states (150 Ω), especially in 9–14 GHz the circular dichroism is nearly 1. With the increase of resistance value, the circular dichroism becomes gradually inconspicuous. When the varistor diodes are at "Off" states (200 MΩ), the circular dichroism almost disappears.

For the purpose of encoding spin-multiplexing holograms based on amplitude distributions, the Rayleigh–Sommerfeld diffraction formula as well as the point source

method are applied [42]. First, the 0/1 amplitude distributions of left-handed and right-handed circularly polarized waves are calculated, in which the phase distributions are considered as uniform. Subsequently, the amplitude distributions of each spin state are combined and each pixel is expressed by binary coding "00", "01", "10", and "11". According to the binary coding distribution, the corresponding meta-atoms are arranged at the predesigned positions. Here, the metasurface hologram contains 60×60 pixels with a period of 6.0 mm in x- and y-directions, which are in accordance with the periodic lengths of meta-atoms. As the proof of principles, the holographic images of "L" and "R" are calculated on the observing plane. The operating frequency is selected at 12 GHz, and the observing plane is set as 300 mm away from the proposed chiral metasurface. The reconstructed images are characterized by electric field scanning technique. The experimental setup is shown in Fig. 5(a), in which a standard horn antenna that can radiate circularly polarized waves and the fabricated metasurface prototype (connected with a DC source) are aligned in an anechoic chamber to reduce the electromagnetic interference. The horn antenna is set far enough with the metasurface prototype to ensure the quasi-plane wave incidence. The scanning probe is placed with a distance of 300 mm to the prototype that can move in the xoy-plane. The probe and the transmitter antenna were connected to two ports of an Agilent N5224A vector network analyzer, respectively. During the measurement, the scanning area is $360 \times 360\,\text{mm}^2$ with a step of 5 mm. The simulated and experimental results are given in Fig. 5(b) and Fig. 5(c), respectively. Here, the bias voltage is applied as 52 V to ensure the varistor diodes in each row are operated at "On" states with the resistance of about 150 Ω. Both the simulated and experimental results manifest the conspicuous reconstructing images of "L" and "R" at the observing plane. The experimental results exhibit good performances with 57.93% and 65.43% imaging pattern efficiency (the energy concentrated in the image area referenced to the total energy on the measured plane), 28.43 and 31.61 peak signal-to-noise ratios (SNR, defined as the peak intensity in the image to the standard deviation of the background noise) for "L" and "R" images, respectively. However, compared with the simulated results, there is a slight deterioration in the experimental image quality, which is mainly caused by

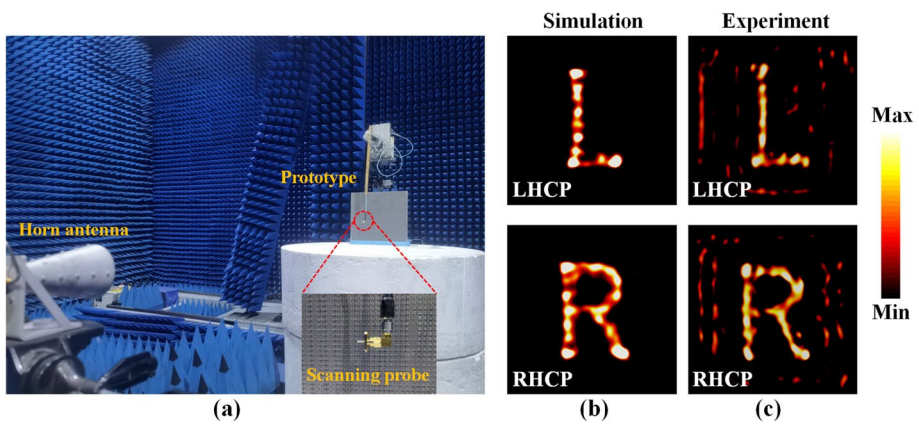

Fig. 5 (**a**) Experimental setup for detecting electric field distributions. (**b**) Simulated results of the intensity distribution at the observed plane. (**c**) Experimental results of the intensity distribution at the observed plane

the fabrication imperfections, the drift of dielectric parameter, and the deviation of active elements.

When the varistor diodes are operated at "Off" states, the amplitude distribution of the chiral metasurface become relatively uniform within the whole aperture. Instead, the phase distribution is similar to the coding metasurface principle with $0/\pi$ distribution according to aforementioned discussion of Fig. 3. Therefore, the far-field scattering patterns in the reflection sphere are governed by passive antenna array theory as [43]:

$$F(\theta,\varphi)=\sum_{m=1}^{N}\sum_{n=1}^{N}\exp\left\{j\left[\varphi_{m,n}+k_0p(m-1/2)\left(\sin\theta\cos\varphi-\sin\theta_i\cos\varphi_i\right)+\ K_0p(n-1/2)\left(\sin\theta\sin\varphi-\sin\theta_i\sin\varphi_i\right)\right]\right\}, \tag{2}$$

where k_0 is the wave vector in free space, $\phi_{m,n}$ is the reflection phase of each coding meta-atom, p is the periodic length of the meta-atom in x- and y-directions, θ_i and ϕ_i are the elevation and azimuth angles, respectively.

Accordingly, it is concluded that the beam scattering effect can be achieved. The far-field scattering patterns under the illumination of left-handed and right-handed circularly polarized waves at 10 GHz, 12 GHz, and 14 GHz are monitored and illustrated in Fig. 6(a)-(c) and Fig. 6(d)-(f), in which the results of metal plate with the same size of proposed chiral metasurface, the results of "On" states and "Off" states are compared. Here, the results at *xoz*-plane are depicted. Obviously, the backward reflection is dramatically reduced when the varistor diodes are turned at "Off" states. Moreover, the side-lobes become larger than the metal plate. The reduction of 16.5 dB, 21.7 dB, and 15.5 dB is obtained for left-handed circularly polarized incidence at 10 GHz, 12 GHz, and 14 GHz. The reduction of 17.1 dB, 19.9 dB, and 14.3 dB is obtained for right-handed circularly polarized incidence at 10 GHz, 12 GHz, and 14 GHz. The differences between left-handed and right-handed circularly polarized reflection are owing to the non-identical coding sequences. It is noticed that the results of varistor diodes are at "On" states also have the slight effect of backward reflection reduction, which is attributed to the uneven distributions of amplitude responses.

To experimentally demonstrate the feasibility of low observable reflection, the reflection characteristics are investigated in anechoic chamber. The experimental setup is shown in Fig. 7(a), in which a pair of horn antennas that connect to the two ports of an

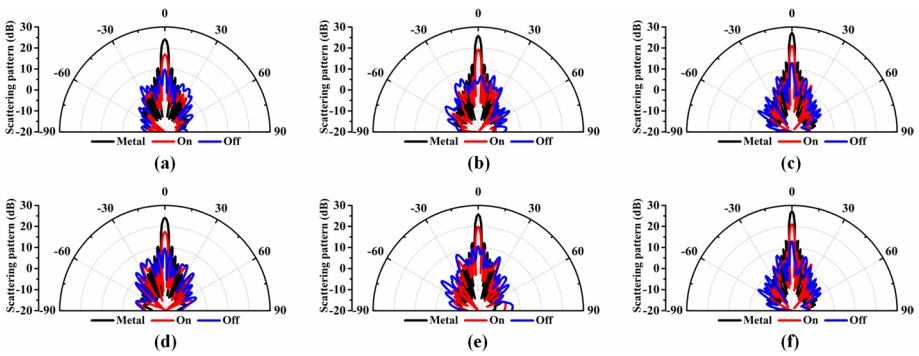

Fig. 6 (**a**)-(**c**) Far-field scattering patterns under the incidence of left-handed circularly polarized waves. (**d**)-(**f**) Far-field scattering patterns under the incidence of right-handed circularly polarized waves

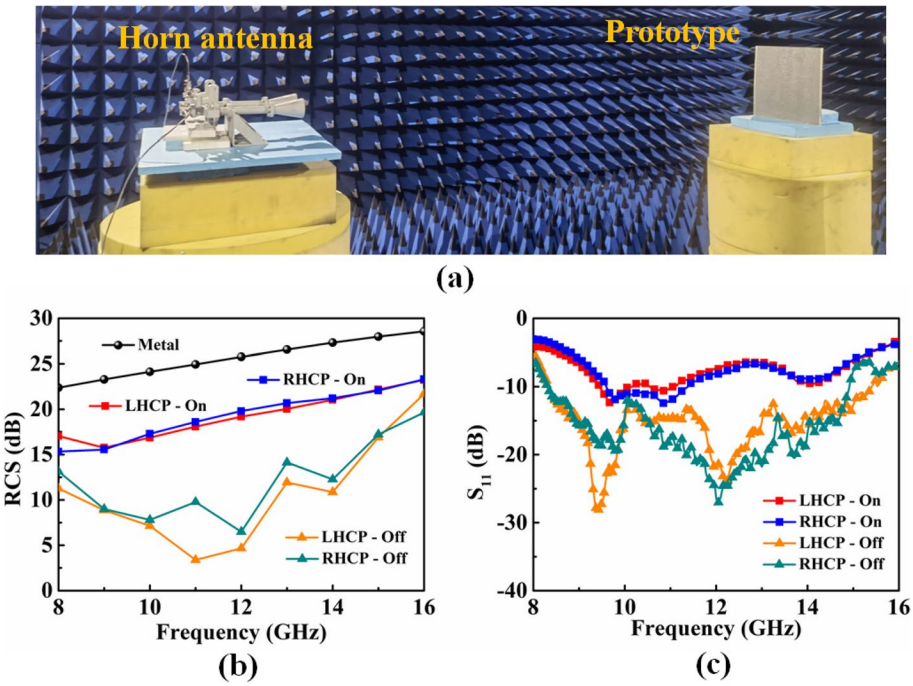

Fig. 7 (**a**) The experimental setup for measuring S_{11}. (**b**) Radar-cross section curves in the range of 8 to 16 GHz. (**c**) S_{11} curves in the range of 8 to 16 GHz

Agilent N5224A vector network analyzer is set far enough to the fabricated chiral metasurface. First of all, as verification and comparison of the low observable characteristics, the simulated radar-cross section (RCS) curves under the incidence of left-handed and right-handed circularly polarized waves are compared in Fig. 7(b). The large RCS reduction effect is achieved for both left-handed and right-handed circularly polarized reflection in 8–16 GHz when the varistor diodes are at "Off" states. For further verification, we have measured the specular reflection of S_{11} in the same frequency band. Compared with the curves of varistor diodes at "On" states, the S_{11} curves of the passive states are lower. Especially in 10–14 GHz, the reduction of specular reflection is more than 15 dB than the metal plate with the same size, which verifies the good low observable reflection characteristics at "Off" states.

Conclusions

We have proposed a generic strategy that can tailor the magnitude of circular dichroism by manipulating different DC bias voltage. By meticulously arranging the proposed four kinds of meta-atoms, a dynamic chiral metasurface driven by bias voltage is fabricated to achieve the functionality integration of spin multiplexing hologram and low observable reflection in microwave regime. The good agreement between numerical simulations and experimental verifications manifests the feasibility of our proposed paradigm. Owing to the concise topological structures, it is inferred that the proposed strategy may be extended to the terahertz or optical frequency by replace the loaded varistor diodes with the phase change materials including Vanadium oxide, $Ge_2Sb_2Te_5$ (GST), and the like.

Furthermore, by properly arranging the resistance value of varistor diode, the more levels of amplitude responses can be theoretically achieved and may apply to the practical fields requiring energy allocations of reradiation waves. In addition, the proposed paradigm is possible to provide spatially varying distributions by further developing the feed systems for independent control in each raw or each pixel with the support of field programmable gate array. In this way, it can further expand and explore the aspects of versatile functionalities/multiple meta-holograms integration. Encouragingly, the proposed strategy can be used to achieve more flourishing functionalities for dynamic control, which may find applications in information encryption, anti-counterfeiting, and other dynamic systems.

Abbreviations

LHCP: Left-handed circular polarization; RHCP: Right-handed circular polarization; PB: PANCHARATAM-Berry; GHz: Gigahertz; PCB: Printed circuit board; F4B: POLY tetra fluoroethylene; DC: Direct current; CST: Computer simulation technology; RCS: Radar-cross section; GST: $Ge_2Sb_2Te_5$; CD: Circular dichroism.

Acknowledgements

Not applicable.

Authors' contributions

H. W., L. H., and R. Z. proposed the idea; H.W. conducted pattern designs and numerical simulations; Z. Q., and Y.L. performed the measurements; R. Z. and H. Z. supported the data for hologram; H. W., Z. Q., L. H., Y. L., H. Z., and H. H. prepared the manuscript; L. H., Y. L., J. Z. and S. Q. supervised the overall projects. H. W., Z. Q., L. H., Y. L., R. Z., and H. Z. analyzed the data and discussed the results. All authors read and approved the final manuscript.

Funding

This work is sponsored by the National Key Research and Development Program of China (2021YFA1401200), Ministry of Science and Technology; the National Natural Science Foundation of China (Grant Nos. 61971437, 92050117, U21A20140); the Beijing Outstanding Young Scientist Program (Grant No. BJJWZYJH01201910007022); the Natural Science Foundation of Shaanxi Province (Grant No.2020JM-342).

Availability of data and materials

The datasets and figures used and analyzed during the current study are available from the corresponding author on reasonable request.

Declarations

Competing interests

The authors declare that they have no competing interests.

Received: 26 January 2022 Accepted: 2 April 2022
Published online: 12 April 2022

References

1. Yu N, Genevet P, Kats MA, Aieta F, Tetienne J, Capasso F, et al. Light propagation with phase discontinuities: generalized laws of reflection and refraction. Science. 2011;334(6054):333–7.
2. Huang L, Chen X, Mühlenbernd H, Zhang H, Chen S, Bai B, et al. Three-dimensional optical holography using a plasmonic metasurface. Nat Commun. 2013;4(1):2808.
3. Yu N, Capasso F. Flat optics with designer metasurfaces. Nat Mater. 2014;13(2):139–50.
4. Lee D, So S, Hu G, Kim M, Badloe T, Cho H, et al. Hyperbolic metamaterials: fusing artificial structures to natural 2D materials. eLight. 2022;2(1).
5. Chen S, Li Z, Liu W, Cheng H, Tian J. From single-dimensional to multidimensional manipulation of optical waves with metasurfaces. Adv Mater. 2019;31(16):1802458.
6. Sun S, Yang K, Wang C, Juan T, Chen WT, Liao CY, et al. High-efficiency broadband anomalous reflection by gradient meta-surfaces. Nano Lett. 2012;12(12):6223–9.
7. Li Z, Hao J, Huang L, Li H, Xu H, Sun Y, et al. Manipulating the wavefront of light by plasmonic metasurfaces operating in high order modes. Opt Express. 2016;24(8):8788–96.
8. Yu S, Li L, Shi G, Zhu C, Shi Y. Generating multiple orbital angular momentum vortex beams using a metasurface in radio frequency domain. Appl Phys Lett. 2016;108(24):241901.
9. Bao Y, Ni J, Qiu C. A minimalist single-layer metasurface for arbitrary and full control of vector vortex beams. Adv Mater. 2019;32(6):1905659.

10. Zhao Y, Belkin MA, Alù A. Twisted optical metamaterials for planarized ultrathin broadband circular polarizers. Nat Commun. 2012;3(1):870.
11. Chen X, Huang L, Mühlenbernd H, Li G, Bai B, Tan Q, et al. Dual-polarity plasmonic metalens for visible light. Nat Commun. 2013;3(1):1198.
12. Jin R, Tang L, Li J, Wang J, Wang Q, Liu Y, et al. Experimental demonstration of multidimensional and multifunctional metalenses based on photonic spin Hall effect. ACS Photonics. 2020;7(2):512–8.
13. Landy NI, Sajuyigbe S, Mock JJ, Smith DR, Padilla WJ. Perfect metamaterial absorber. Phys Rev Lett. 2008;100(20):207402.
14. Huang K, Dong Z, Mei S, Zhang L, Liu Y, Liu H, et al. Silicon multi-meta-holograms for the broadband visible light. Laser Photonics Rev. 2016;10(3):500–9.
15. Yifat Y, Eitan M, Iluz Z, Hanein Y, Boag A, Scheuer J. Highly efficient and broadband wide-angle holography using patch-dipole nanoantenna reflectarrays. Nano Lett. 2014;14(5):2485–90.
16. Zhou H, Wang Y, Li X, Wang Q, Wei Q, Geng G, et al. Switchable active phase modulation and holography encryption based on hybrid metasurfaces. Nanophotonics. 2020;9(4):905–12.
17. Chang X, Bian L, Zhang J. Large-scale phase retrieval. eLight. 2021;1(4).
18. Probst PT, Mayer M, Gupta V, Steiner AM, Zhou Z, Auernhammer GK, et al. Mechano-tunable chiral metasurfaces via colloidal assembly. Nat Mater. 2021;20(7):1024–8.
19. Zheng C, Li J, Li J, Yue Z, Wang S, Li M, et al. All-silicon chiral metasurfaces and wavefront shaping assisted by interference. Sci China Phys Mech. 2021;64(11):114212.
20. Zhang F, Pu M, Li X, Gao P, Ma X, Luo J, et al. All-Dielectric metasurfaces for simultaneous giant circular asymmetric transmission and wavefront shaping based on asymmetric photonic spin-orbit interactions. Adv Funct Mater. 2017;27(47):1704295.
21. Zhu AY, Chen WT, Zaidi A, Huang Y, Khorasaninejad M, Sanjeev V, et al. Giant intrinsic chiro-optical activity in planar dielectric nanostructures, Light: Sci. Appl. 2018;7(2):17158.
22. Semnani B, Flannery J, Maruf RA, Bajcsy M. Spin-preserving chiral photonic crystal mirror, Light: Sci. Appl. 2020;9(1):23.
23. Wang Z, Jing L, Yao K, Yang Y, Zheng B, Soukoulis CM, et al. Origami-based reconfigurable metamaterials for tunable chirality. Adv Mater. 2017;29(27):1700412.
24. Li W, Coppens ZJ, Besteiro LV, Wang W, Govorov AO, Valentine J. Circularly polarized light detection with hot electrons in chiral plasmonic metamaterials. Nat Commun. 2015;6:8379.
25. Kang L, Lan S, Cui Y, Rodrigues SP, Liu Y, Werner DH, et al. An active metamaterial platform for chiral responsive optoelectronics. Adv Mater. 2015;27(29):4377–83.
26. Wang Z, Cheng F, Winsor T, Liu Y. Optical chiral metamaterials: a review of the fundamentals, fabrication methods and applications. Nanotechnology. 2016;27(41):412001.
27. Jing L, Wang Z, Yang Y, Zheng B, Liu Y, Chen H. Chiral metamirrors for broadband spin-selective absorption. Appl Phys Lett. 2017;110:231103.
28. Kang L, Rodrigues S, Taghinejad M, Lan S, Lee K, Liu Y, et al. Preserving spin states upon reflection: linear and nonlinear responses of a chiral meta-mirror. Nano Lett. 2017;17(11):7102–9.
29. Kwon H, Faraon A. NEMS-tunable dielectric chiral metasurfaces. ACS Photonics. 2021;8(10):2980–6.
30. Xu Y, Li Q, Zhang X, Wei M, Xu Q, Wang Q, et al. Spin-decoupled multifunctional metasurface for asymmetric polarization generation. ACS Photonics. 2019;6(11):2933–41.
31. Gansel JK, Thiel M, Rill MS, Decker M, Bade K, Saile V, et al. Gold helix photonic metamaterial as broadband circular polarizer. Science. 2009;325(5947):1513–5.
32. Dietrich K, Lehr D, Helgert C, Tünnermann A, Kley E. Circular Dichroism from Chiral Nanomaterial Fabricated by On-Edge Lithography. Adv Mater. 2012;24(44):OP321–5.
33. Wang Z, Jia H, Yao K, Cai W, Chen H, Liu Y. Circular dichroism metamirrors with near-perfect extinction. ACS Photonics. 2016;3(11):2096–101.
34. Cui T, Qi M, Wan X, Zhao J, Cheng Q. Coding metamaterials, digital metamaterials and programmable metamaterials, Light: Sci. Appl. 2014;3(10):e218.
35. Zhang L, Wang ZX, Shao RW, Shen JL, Chen XQ, Wan X, et al. Dynamically realizing arbitrary multi-bit programmable phases using a 2-bit time-domain coding metasurface. IEEE T Antenn Propag. 2019;68(4):2984–92.
36. Zhang L, Chen X, Shao R, Dai J, Cheng Q, Castaldi G, et al. Breaking reciprocity with space-time-coding digital metasurfaces. Adv Mater. 2019;31(41):1904069.
37. Dai JY, Yang LX, Ke JC, Chen MZ, Tang W, Li X, et al. High-efficiency synthesizer for spatial waves based on space-time-coding digital metasurface. Laser Photonics Rev. 2020;14(6):1900133.
38. Huang CX, Zhang J, Cheng Q, Cui TJ. Polarization Modulation for Wireless Communications Based on Metasurfaces. Adv Funct Mater. 2021;31(36):2103379.
39. Chen K, Zhang N, Ding G, Zhao J, Jiang T, Feng Y. Active anisotropic coding metasurface with independent real-time reconfigurability for dual polarized waves. Adv Mater Technol. 2020;5(2):1900930.
40. Jing L, Wang Z, Maturi R, Zheng B, Wang H, Yang Y, et al. Gradient chiral metamirrors for spin-selective anomalous reflection. Laser Photonics Rev. 2017;11(6):1700115.
41. Wang H, Jing Y, Li Y, Huang L, Feng M, Yuan Q, et al. Tailoring circular dichroism for simultaneous control of amplitude and phase via ohmic dissipation metasurface. Adv Opt Mater. 2021;9(12):2100140.
42. Li B, Li X, Zhao R, Wang G, Han W, Zhao B, et al. Polarization multiplexing terahertz metasurfaces through spatial femtosecond laser-shaping fabrication. Adv Opt Mater. 2021;8(12):2000136.
43. Liu S, Cui TJ, Zhang L, Xu Q, Wang Q, Wan X, et al. Convolution operations on coding metasurface to reach flexible and continuous controls of terahertz beams. Adv Sci. 2016;3(10):1600156.

Publisher's Note

Springer Nature remains neutral with regard to jurisdictional claims in published maps and institutional affiliations.